ELSEVIER

Journal of Power Sources 97–98 (2001) 518–524

JOURNAL OF POWER SOURCES

www.elsevier.com/locate/jpowsour

Recent investigations on thin films and single particles of transition metal oxides for lithium batteries

I. Uchida*, M. Mohamedi, K. Dokko, M. Nishizawa, T. Itoh, M. Umeda

Department of Applied Chemistry, Graduate School of Engineering, Tohoku University, 07 Aramaki Aoba, Aoba-Ku, Sendai 980-8579, Japan

Received 1 June 2000; accepted 22 January 2001

Abstract

Various aspects in the lithium battery field have been explored in our group: (i) uniform and dense thin films of $LiMn_2O_4$ up to 0.5 μm thickness have been synthesized by electrostatic spray deposition (ESD). The electrochemical properties of these films were investigated by cyclic voltammetry and impedance spectroscopy under a variety of experimental conditions. (ii) The kinetic and transport properties of lithium insertion/extraction of numerous sphere-shaped single particles have been also evaluated by transient techniques as well as by ac-impedance spectroscopy. (iii) Electrochemical quartz crystal microbalance (EQCM) technique was employed to study the low capacity fading of $LiMn_2O_4$ at elevated temperatures in $LiPF_6$ containing solutions. It has been confirmed that this phenomenon is due to the manganese dissolution promoted by acidic species (HF) originated from the reaction of $LiPF_6$ with water. (iv) Alternative materials were sought to replace the actual $LiCoO_2$ or $LiMn_2O_4$. Among them: $Li_{1.1}Mn_{1.9}O_4$, $LiNi_{0.85}Co_{0.15}O_2$ and $Li_{1.10}Mn_{1.852}Cr_{0.048}O_4$. Interestingly, $Li_{1.10}Mn_{1.852}Cr_{0.048}O_4$ exhibited no significant capacity fading even in the 1 M $LiPF_6$/PC–EC (1:1) solution at 50°C upon 50 cycles of charge/discharge.

Keywords: Lithium battery; Thin films; Microelectrodes; Stability

1. Introduction

Intense research program dealing with several aspects related to battery systems is going on in our laboratory. Part of this program is to develop both new anode and cathode materials that would bring down the cost and improve the performance of the actual batteries. Other argued phenomena for instance lithium insertion/extraction mechanism and manganese dissolution are also being investigated in our group. Particularly, several novel techniques to characterize the insertion/extraction processes have been proposed [1–11]. The primary objective of this paper is to present an overview of some of our recent studies and techniques.

2. Thin film electrodes

Progress in the miniaturization of electronic devices have reduced the current and power requirements to extremely low levels, making possible the use of thin film microbatteries as a power sources for some of these devices. To integrate such batteries into the electronics at the chip level, it is mandatory to prepare thin film components of the battery systems using process compatible with microelectronics fabrication technologies. For that purpose, we adopted the electrostatic spray deposition (ESD) technique, and achieved the synthesis of a uniform and dense film of spinel $LiMn_2O_4$ up to 0.5 micrometer thick. The full descriptions of the ESD set-up and its working principles are reported elsewhere [1,12,13].

The electrochemistry of these $LiMn_2O_4$ thin films was investigated by cyclic voltammetry (CV) and electrochemical impedance spectroscopy (EIS) in various experimental conditions of electrolyte, temperature, and thickness. Typical CVs and EIS spectra of thin films $LiMn_2O_4$ (ca. 0.1 μm) recorded in various electrolyte systems at 50°C are illustrated in Figs. 1 and 2, respectively. It is very significant that the CVs of the electrodes in the three solutions are very similar in shape. It is noticed in Fig. 2, that $LiBF_4$/PC–EC solution yields lower interfacial impedance [14]. The EIS data have been modeled using an equivalent circuit approach following rigorous criteria [2]. An excellent fit was found between measured data and the derived model, comprising Li^+ migration through surface layer, potential-dependent charge transfer resistance, semiinfinite Warburg-type

* Corresponding author. Tel.: +81-22-217-7220; fax: +81-22-214-8646.
E-mail address: uchida@est.che.tohoku.ac.jp (I. Uchida).

0378-7753/01/$ – see front matter
PII: S0378-7753(01)00724-8

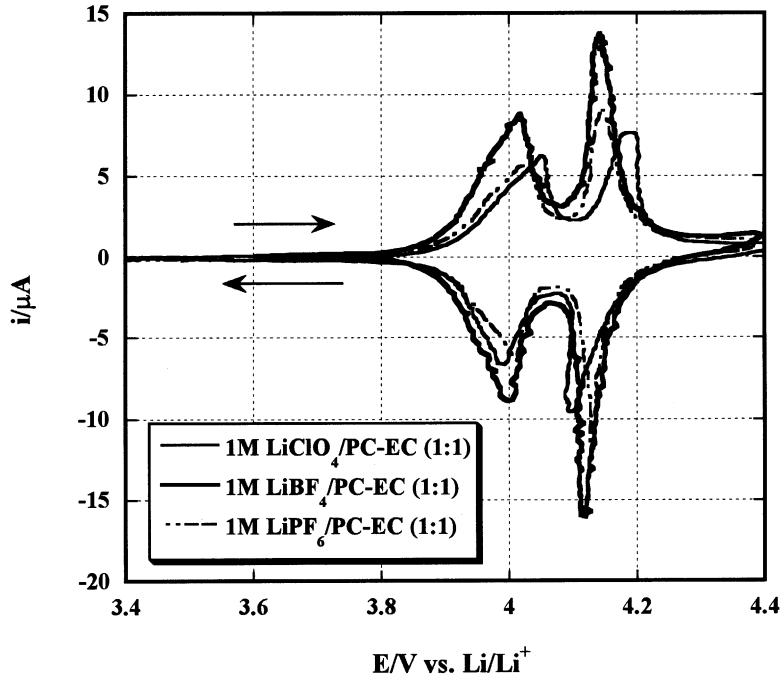

Fig. 1. Cyclic voltammograms (third cycle) of ESD synthesized thin film $LiMn_2O_4$ (0.1 μm in thickness) electrodes measured at 0.5 mV/s in the three PC–EC (1:1) salt solutions at 50°C.

element, reflecting solid state Li^+ ion diffusion and a finite space Warburg-type element, describing both diffusion and accumulation of lithium at the very low frequency. The diffusion coefficient of the lithium versus E curves for all electrodes in the three salt solutions are very similar and shows peak shaped functions with minima at the CV peak potentials. The D_{Li}-values varied from 10^{-9} to 10^{-10} cm^2/s within 3.7 and 4.4 V range at 50°C.

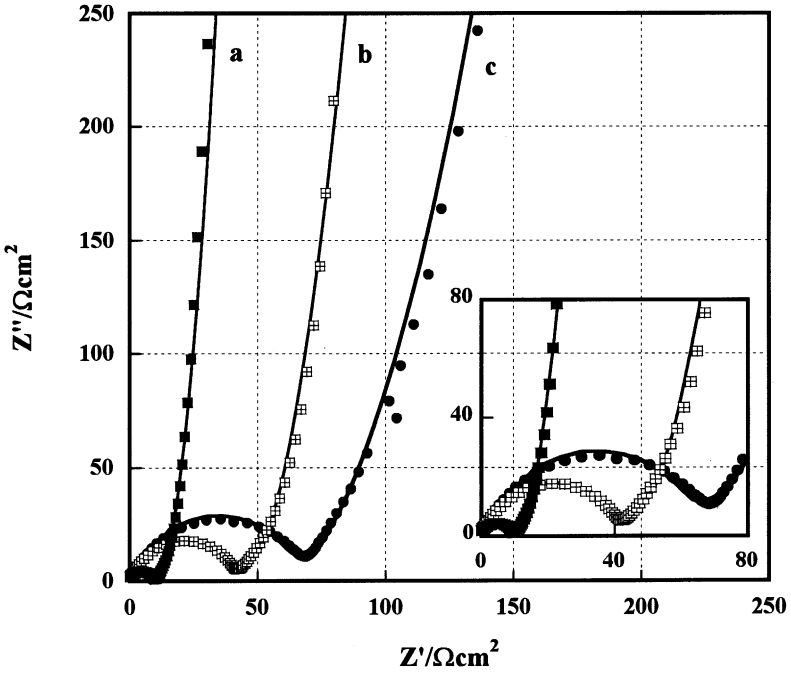

Fig. 2. Nyquist plots obtained from ESD synthesized thin film $LiMn_2O_4$ (0.1 μm in thickness) electrodes at 4.02 V vs. Li/Li^+ in the PC–EC (1:1) salt solutions at 50°C. (a) $LiBF_4$ 1 M solution, (b) $LiClO_4$ 1 M solution, and (c) $LiPF_6$ 1 M solution. Simulated curves are shown as solid lines.

3. Microelectrode techniques

With the microelectrode techniques, one can obtain intrinsic responses solely from the reaction between the active material and the electrolyte. In other words, the results are not complicated by the influence of the binders and conductive additives necessary for the fabrication of porous electrodes. Furthermore, because of the small size of the electrode, the contribution of the resistive polarization and the capacitive current due to the double layer capacity are greatly reduced.

A microelectrode technique for battery materials has been developed in our group [3–11] and successfully employed for the evaluation of the kinetic and transport properties of lithium insertion/extraction of a particle with a diameter of 10–100 μm. We were able to perform transient as well as EIS methods on sphere shaped single particles of $LiCoO_2$, $LiMn_2O_4$, $LiNiO_2$, $Li_{1.1}Mn_{1.9}O_4$, $LiNi_{0.85}Co_{0.15}O_2$ and $Li_{1.10}Mn_{1.852}Cr_{0.048}O_4$.

Fig. 3 presents an example of cyclic voltammogram obtained for the $LiCoO_2$ single particle of 12 μm diameter [15]. The CV was performed at a slow scan rate of 1 mV/s. The voltammogram is characterized by three sets well-defined current peaks. The main lithium intercalation and deintercalation peaks appeared at the potentials of 3.88 and 3.91 V, respectively. Two high voltage peaks observed above 4 V that may results from phase transition between ordered and disordered lithium ion arrangements in the CoO_2 framework [16].

Electrochemical impedance spectroscopy (EIS) has been also applied to the single $LiCoO_2$ particle during lithium extraction process [15]. The shape of impedance spectra was found to depend on the applied potential. At potentials below 3.80 V (i.e. in the non-faradaic region) the impedance spectra demonstrated a blocking behavior of the electrode. Within 3.80–3.90 V potential range that corresponds to the main deintercalation/intercalation, the impedance spectra showed a complicated behavior. The spectra exhibited a depressed semi-circle likely consisting of two or more overlapped semi-circles followed by a Warburg-type element at low frequencies. For potential >3.90 V, the impedance changed to a simplest shape as shown in Fig. 4. It was composed of a single semi-circle in the high-frequency region followed by a Warburg-type element, which reflects the solid-state diffusion of lithium ions into the $LiCoO_2$ matrix. At the very low frequencies, the imaginary versus the real part plots became steep approaching nearly 90° which reflects capacitive behavior (Fig. 4). This capacitive behavior simply relates to the intercalation capacity of the electrode, which is strongly potential dependent.

4. Manganese dissolution

An important problem standing in the way of wider use of the $LiMn_2O_4$ as a positive electrode is its poor performance at elevated temperatures. This aspect has been widely addressed lately, and measures to tackle it have been proposed. There is no consensus as to the reasons for this unfortunate phenomenon, and the following causes have been postulated: (i) spinel dissolution; (ii) structural instability in the charged state; (iii) electrolyte decomposition; and (iv) Jahn–Teller effect.

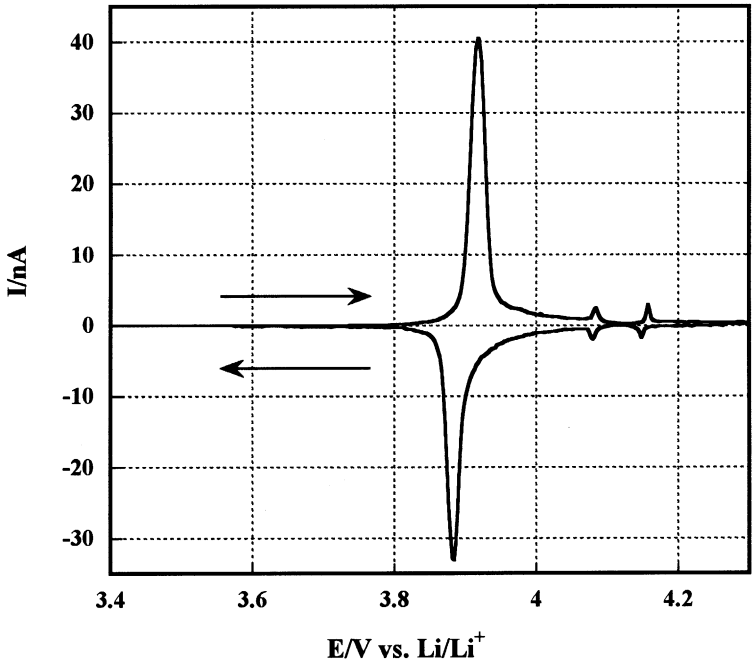

Fig. 3. Cyclic voltammogram (third cycle) obtained for a $LiCoO_2$ single sphere-shaped particle (12 μm in diameter) run at 1 mV/s in the 1 M $LiClO_4$/PC–EC (1:1) salt solution at 25°C.

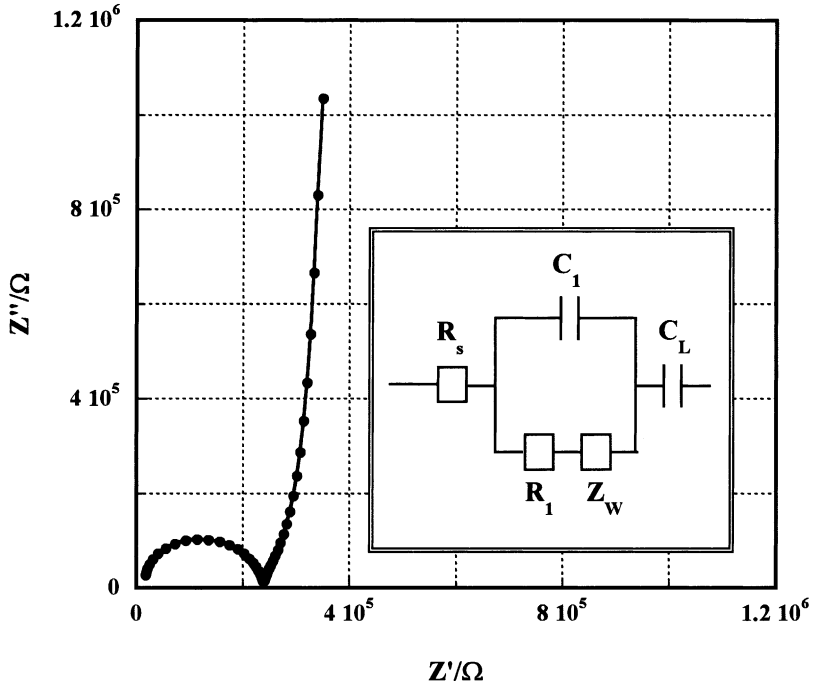

Fig. 4. Nyquist plot obtained from $LiCoO_2$ single sphere-shaped particle (12 μm in diameter) at 4.20 V vs. Li/Li^+ in the 1 M $LiClO_4$/PC–EC (1:1) salt solution at 25°C. Insert shows the equivalent circuit used for the simulation of impedance data recorded at potentials greater than 3.90 V. R_s is the solution resistance, R_1 the charge transfer resistance, C_1 is the total interfacial capacity, Z_W is the Warburg impedance element and C_L represents the intercalation capacity of the electrode. Simulated curve is shown as solid line.

In $LiPF_6$ containing solutions, manganese dissolution is believed to be responsible for the low capacity fading of $LiMn_2O_4$ at elevated temperatures [17–20]. The protons arise from HF, which originates with the hydrolysis of lithium salt ($LiPF_6$) and thus depends critically of lithium salt purity.

The microelectrode technique has been applied to a single particle of $LiMn_2O_4$ in 1 M $LiPF_6$/PC–EC (1:1) solution at 50°C [21]. Multi-cyclic voltammetry showed a significant decrease in capacity (ca. 25% decrease upon 50 cycles) (Fig. 5). This was attributed to the dissolution of manganese

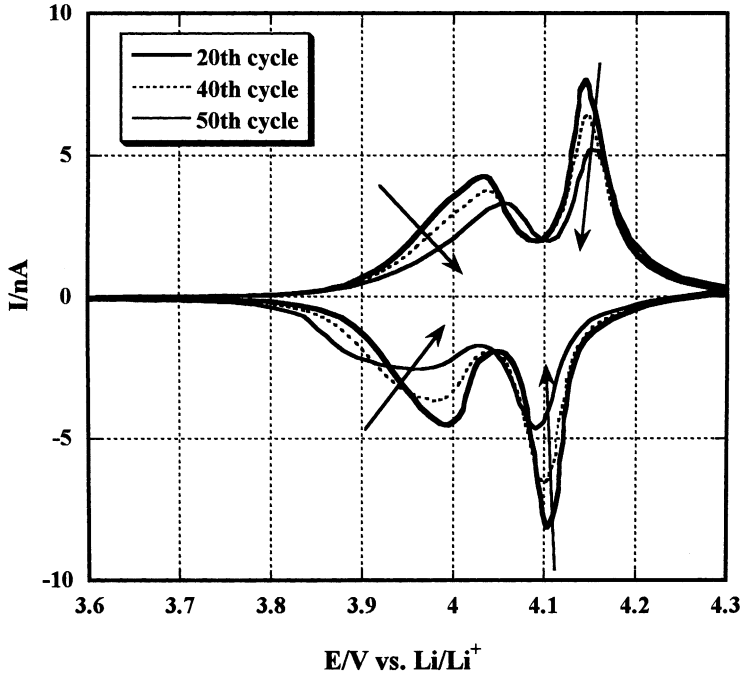

Fig. 5. First 50 cyclic voltammograms obtained for a $LiMn_2O_4$ single sphere-shaped particle (14 μm in diameter) run at 0.5 mV/s in the 1 M $LiPF_6$/PC–EC (1:1) salt solution at 50°C.

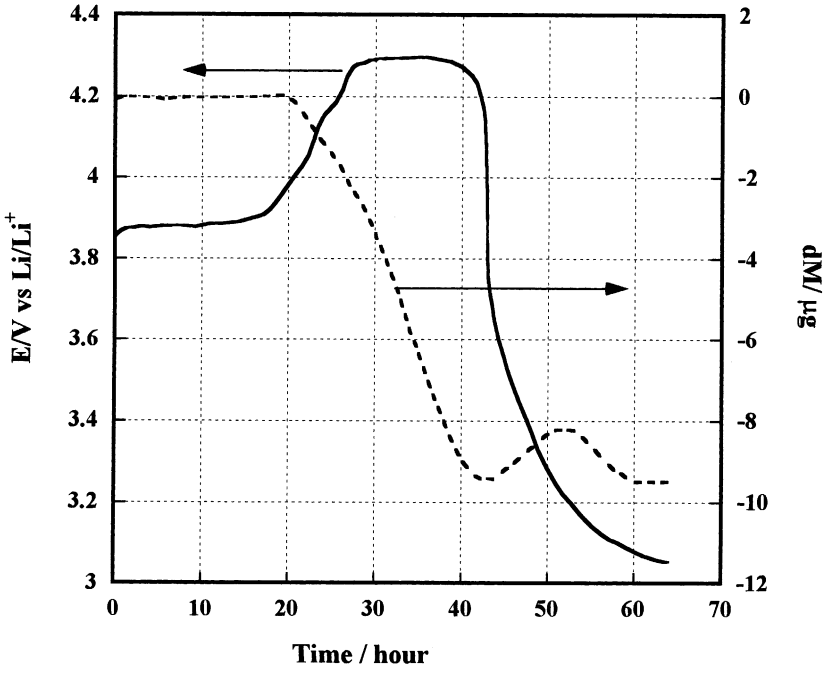

Fig. 6. The time-courses of open-circuit potential and mass of ESD synthesized thin film $LiMn_2O_4$ upon storage at 50°C in 1 M $LiPF_6$/PC–EC (1:1) salt solution. The initial mass of $LiMn_2O_4$ was about 10 μg.

oxide promoted by acidic species (HF) originated from the reaction of $LiPF_6$ with water. We have confirmed subsequently, the role of water in the dissolution process.

The manganese dissolution was further investigated by means electrochemical quartz crystal microbalance (EQCM) technique on thin $LiMn_2O_4$ films. This technique enables a direct measurement of the manganese dissolution process. The open circuit voltage and mass of $LiMn_2O_4$ were followed upon exposure in a 1 M $LiPF_6$/PC–EC (1:1) solution at 50°C (Fig. 6) [22]. After 20 h of storage, the mass started to decrease. This mass decrease is obviously due to the dissolution of the manganese oxide. Photographs of the

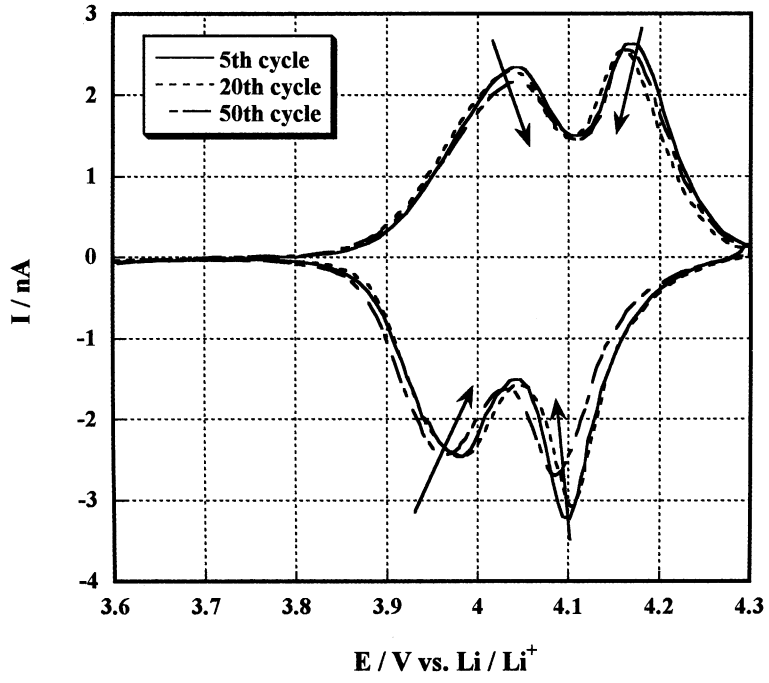

Fig. 7. First 50 cyclic voltammograms obtained for a $Li_{1.10}Mn_{1.852}Cr_{0.048}O_4$ single sphere-shaped particle (12 μm in diameter) run at 0.5 mV/s in the 1 M $LiPF_6$/PC–EC (1:1) salt solution at 50°C.

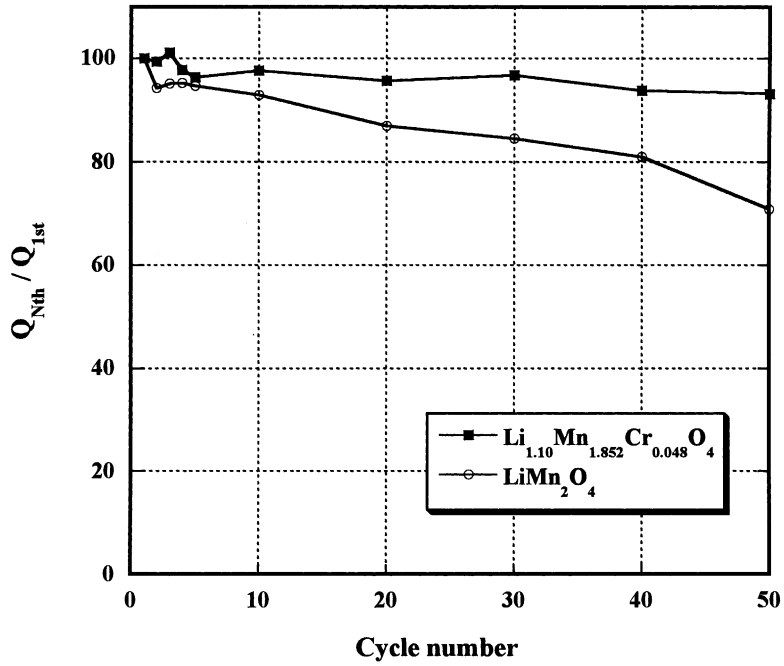

Fig. 8. Discharge capacities as function of cycle number for $LiMn_2O_4$ and $Li_{1.10}Mn_{1.852}Cr_{0.048}O_4$ single particles in 1 M $LiPF_6$/PC–EC (1:1) salt solution at 50°C.

electrode prior and after storage showed that all the $LiMn_2O_4$ has vanished. Other salient feature of Fig. 6 is that the OCP-value increased up to 4.3 V and sustained at this potential for about 14 h during the course of dissolution of the manganese oxide. All these results are very likely to support that the manganese dissolution induced by the H^+ attack proceeds with the formation of l-MnO_2 phase at the surface according to the following reaction scheme:

$$2H_2O + 2PF_6^- \rightarrow 2POF_3 + 4H^+ + 6F^- \quad (1)$$

$$2LiMn_2O_4 + 4H^+ \rightarrow 3\lambda - MnO_2 + Mn^{2+} + 2H_2O \quad (2)$$

Thus, the disproportionation reaction of $LiMn_2O_4$ (Eq. 2) associated with the protons generated by reaction 1 would make the manganese dissolution process autocatalytic in nature.

5. Cathode materials

As part of a comprehensive program on the science and technology of the Li-ion batteries, we have carried out studies on the capacity improvement of various cathodes with single/multiple doping. Transition metal oxides such as $Li_{1.1}Mn_{1.9}O_4$, $LiNi_{0.85}Co_{0.15}O_2$, and $Li_{1.10}Mn_{1.852}Cr_{0.048}O_4$ (spherical beads supplied from Nikki Chemicals Co.) have been studied at 50°C using the microelectrode technique [21].

Interesting result concerns the $Li_{1.10}Mn_{1.852}Cr_{0.048}O_4$ (Fig. 7). This material exhibited no significant capacity fading even in the 1 M $LiPF_6$/PC–EC (1:1) solution at 50°C upon 50 cycles of charge/discharge (Fig. 8). It is not clear how the doping has stabilized the spinel structure, but it might be suggested that because of Cr–O bond is stronger than Mn–O bond.

6. Conclusions

In this work, we presented a summary of our recent achievements in the *R* and *D* of the lithium ion batteries. Our techniques provide a quick evaluation for the insertion/extraction materials without having to employ a whole cell construction. Further details, complete analysis, and interpretation of the results pointed out in this lecture will be submitted for publication in the very near future.

Acknowledgements

This work was partly supported by Grant-in-Aids for Scientific Research on Priority Area for ''Electrochemistry of Ordered Interfaces'' from the Ministry of Education Science, Sports and Culture, Japan and by the Lithium Battery Energy Storage Technology Research Association (LIBES), Japan.

References

[1] M. Nishizawa, T. Uchiyama, K. Dokko, K. Yamada, T. Matsue, I. Uchida, Bull. Chem. Soc. Jpn. 71 (1998) 2011.
[2] M. Mohamedi, D. Takahashi, T. Uchiyama, T. Itoh, M. Nishizawa, I. Uchida, J. Power Sources 93 (2001) 93–103.

[3] S. Waki, K. Dokko, T. Itoh, M. Nishizawa, T. Abe, I. Uchida, J. Solid State Electrochem. 4 (2000) 205.
[4] M. Nishizawa, H. Koshika, I. Uchida, J. Phys. Chem. B 103 (1999) 192.
[5] M. Nishizawa, I. Uchida, Electrochemistry 67 (1999) 420.
[6] M. Nishizawa, I. Uchida, Electrochim. Acta 44 (1999) 3629.
[7] M. Nishizawa, R. Hashitani, T. Itoh, T. Matsue, I. Uchida, Electrochem. Solid. State Lett. 1 (1998) 10.
[8] K. Dokko, M. Nishizawa, I. Uchida, Denki Kagaku 66 (1998) 1188.
[9] I. Uchida, H. Fujiyoshi, S. Waki, J. Power Sources 68 (1997) 139.
[10] T. Nishina, H. Ura, I. Uchida, J. Electrochem. Soc. 144 (1997) 1273.
[11] H. Ura, T. Nishina, I. Uchida, J. Electroanal. Chem. 396 (1995) 169.
[12] A.A. van Zomeron, E.M. Kelder, J.C. Marijnissen, J. Schoonman, J. Aerosol. Sci. 25 (1994) 1229.
[13] C. Chen, E.M. Kelder, P.J.J.M. van der Put, J. Schoonman, J. Mater. Chem. 6 (1996) 765.
[14] M. Mohamedi, D. Takahashi, T. Itoh, M. Umeda, I. Uchida, in preparation.
[15] K. Dokko, Y. Fujita, M. Mohamedi, T. Itoh, M. Umeda, I. Uchida, in press.
[16] J.N. Reimers, J.R. Dahn, J. Electrochem. Soc. 139 (1992) 2091.
[17] D.H. Jang, Y.J. Shin, S.M. Oh, J. Electrochem. Soc. 143 (1996) 2204.
[18] D.H. Jang, S.M. Oh, J. Electrochem. Soc. 144 (1997) 3342.
[19] D.H. Jang, S.M. Oh, Electrochim. Acta 43 (1998) 1023.
[20] G.G. Amatucci, A. Blyr, C. Sigala, P. Alfonse, J.M. Tarascon, Solid State Ion. 104 (1999) 13.
[21] K. Dokko, S. Horikoshi, T. Itoh, M. Nishizawa, M. Mohamedi, I. Uchida, J. Power Sources 90 (2000) 109–115.
[22] T. Uchiyama, M. Nishizawa, T. Itoh, I. Uchida, J. Electrochem. Soc 147 (6) (2000) 2057.